Particle Nucleation in the Tropical Boundary Layer and Its Coupling to Marine Sulfur Sources

A. D. Clarke,* D. Davis, V. N. Kapustin, F. Eisele, G. Chen, I. Paluch, D. Lenschow, A. R. Bandy, D. Thornton, K. Moore, L. Mauldin, D. Tanner, M. Litchy, M. A. Carroll, J. Collins, G. Albercook

New particle formation in a tropical marine boundary layer setting was characterized during NASA's Pacific Exploratory Mission–Tropics A program. It represents the clearest demonstration to date of aerosol nucleation and growth being linked to the natural marine sulfur cycle. This conclusion was based on real-time observations of dimethylsulfide, sulfur dioxide, sulfuric acid (gas), hydroxide, ozone, temperature, relative humidity, aerosol size and number distribution, and total aerosol surface area. Classic binary nucleation theory predicts no nucleation under the observed marine boundary layer conditions.

Condensation nuclei (CN) concentrations over remote marine regions generally exhibit remarkable stability, typically being several hundred per cubic centimeter (*1, 2*) even though cloud processes and precipitation rapidly deplete the CN population. This implies a source that continually restores this population, the origin of which remains poorly understood. Oxidation of gaseous oceanic sulfur emissions in the form of dimethylsulfide (DMS) has been proposed as a potentially important source (*3, 4*). Although some results suggest its importance through gas-to-particle conversion (GPC) in the form of nucleation (*5–8*), other observations indicate otherwise. For example, in the boundary layer (BL), where typically large aerosol surface areas are present, most GPC is believed to involve growth in preexisting aerosol rather than formation of new particles (*2, 9–13*). Thus, most models predict nucleation to be unimportant in this setting (*13, 14*), suggesting instead that it would be favored at high altitudes where both the temperature and aerosol surface area are substantially lower (*9, 14*). Understanding aerosol formation and growth to sizes effective as cloud condensation nuclei is a critical element in improving our ability to assess the potential role of aerosols in climate forcing (*15*). Here we present near-surface airborne results, which place constraints on both particle properties and levels of gas-phase sulfur species and thus challenge current models.

NASA's Pacific Exploratory Mission–Tropics A (PEMT) instrumentation aboard the NASA P3-B aircraft enabled extensive characterization of aerosols, major gas-phase sulfur species, and photochemically active compounds. The aerosol instrumentation (*16*) allowed for evaluation of the size and number distribution, total aerosol surface area, and percentage of refractory material present. The gas-phase instrumentation provided continuous measurements of the key species OH, H_2SO_4, SO_2, and DMS as well as CO, H_2O, NO, O_3, nonmethane hydrocarbons (NMHCs), ultraviolet (UV) irradiance, and numerous meteorological parameters (*17*).

On 23 September 1996, the P3-B flew north from Quayaquil, Ecuador (flight 19), with the objective of examining chemical processes over a marine region just to the south of 8°N. This was thought to be a region potentially rich in DMS emissions. Equally interesting, this region also defined the eastern end of the intertropical convergence zone (ITCZ) and had recently experienced significant deep convection. Near 8°N the aircraft descended to about 160 m for a 1-hour (360 km) BL leg in westerly surface winds off the west coast of Panama (from 8°N 86°W to 5.5°N 85°W). The vertical profile included multilayer clouds and a wet adiabatic lapse rate below 1.3 km. The near-surface layer was dry adiabatic below 280 m on descent and below 180 m on the ascent. The 160-m leg had broken low clouds with relative humidity (RH) near 94% ± 3% but with frequent small clear areas that increased toward the end. A few brief periods of precipitation lasting 10 to 50 s were also encountered.

Aerosol surface area, ultrafine CN (UCN), the CN/UCN ratio (*16*), and H_2SO_4(g) temporal profiles observed during the BL run have been divided into five distinct regions as shown in Fig. 1, A and B. These observations are closely linked to the dynamic changes in the size distributions shown in Fig. 1C. Region 1 reveals evidence of earlier nucleation with nuclei reaching 20 nm. Region 2 is seen having low surface area and high H_2SO_4(g) favorable to the onset of nucleation. Region 3 has low surface area and depleted sulfuric acid and a low CN/UCN ratio, indicating that nucleation is under way (see below). Region 4 has the highest concentrations of nuclei after a nuclear event, and region 5 shows no evidence of recent nucleation.

Expanding the time scale (Fig. 2) suggests that the most active nucleation (lowest CN/UCN ratio) occurred over a distance of 20 km in region 3 in association with the lowest temperature for the leg and during which time a small shower occurred. The lowered temperature (Fig. 2A) and strong inflection in the CN/UCN ratio between regions 3 and 4 are consistent with recent or ongoing nucleation early in region 3. Near the end of region 3 and throughout region 4 the temperature increase is associated with decreasing concentrations and aerosol growth (Fig. 1C). During the period of lowest temperatures and highest UCN, the O_3 concentrations remained below 5 parts per billion by volume (ppbv), indicating that the air parcel and its newly formed nuclei originated below 1.3 km. (Note that O_3 concentrations increased rapidly to 25 ppbv at altitudes near 1.6 km.)

The coupling between DMS and gas-to-particle conversion via nucleation was explored through model simulations (*18*), as constrained by observational data for the most critical species and parameters. These included: DMS, OH, SO_2, H_2SO_4, UCN, CN, total aerosol surface area, temperature (*T*), and RH. The local DMS sea-to-air flux was estimated at 5.7 $\mu mol \cdot m^{-2} \cdot day^{-1}$ and was derived with a mass balance–photochemical modeling approach (*19–21*). This estimate was constrained with observational DMS data, and therefore a high degree of correspondence was expected and found between the observed and simulated values of DMS (Fig. 3). This flux estimate is consistent with values for other high-productivity regions in the Pacific (*20, 22–25*). The link between DMS and SO_2 was based on a chemical mechanism derived in previous work (*26*)

A. D. Clarke, V. N. Kapustin, K. Moore, M. Litchy, School of Ocean and Earth Science and Technology, University of Hawaii, Honolulu, HI, USA. D. Davis, F. Eisele, G. Chen, School of Earth and Atmospheric Sciences, Georgia Institute of Technology, Atlanta, GA, USA. F. Eisele, L. Mauldin, D. Tanner, Atmospheric Chemistry Division, National Center for Atmospheric Research, Boulder, CO, USA. I. Paluch and D. Lenschow, National Center for Atmospheric Research, Boulder, CO, USA. A. R. Bandy and D. Thornton, Department of Chemistry, Drexel University, Philadelphia, PA, USA. M. A. Carroll and G. Albercook, Atmospheric, Oceanic, and Space Sciences, University of Michigan Ann Arbor, MI, USA. J. Collins, NASA Langley Research Center, Hampton, VA, USA.

*To whom correspondence should be addressed.

and constrained by observational data (OH, DMS, and SO_2). In these simulations both the efficiency factor (EF) for conversion of DMS to SO_2 and the first-order loss of SO_2 (aerosol scavenging and cloud and ocean surface loss) were key adjustable parameters fixed at values of 0.7 and 1.3×10^{-5} s^{-1}, respectively, and derived from other sulfur field studies (*20, 27*). As shown in Fig. 3, good agreement was found between predicted and observed SO_2.

A satisfactory coupling of DMS to new particle formation also requires that the observed SO_2 be capable of sustaining the observed $H_2SO_4(g)$. In these simulations the SO_2/OH reaction was taken to be the major source of H_2SO_4. The major H_2SO_4 sink was taken to be scavenging by the measured aerosol surface area with a H_2SO_4 sticking coefficient (α) of 0.6 ± 0.3, a value estimated from other tropical field data (*20*). During flight 19, the resulting formation rate for $H_2SO_4(g)$ ranged from an early-morning value of 10^2 molecules per cubic centimeter per second to a near-noon maximum of about 10^4 molecules per cubic centimeter per second. For the time period of the nucleation event at 14:00 hours, the value was 7.7×10^3 molecules per cubic centimeter per second.

The above evaluation of the steady-state mixing ratio for H_2SO_4 requires specification of aerosol total surface area. We ran two scenarios involving fixed surface areas of 75 and 13 $\mu m^2/cm^3$. These represent a minimum wet surface area for the in-cloud case and a median value for between-cloud conditions found during the BL flight leg. The corresponding $H_2SO_4(g)$ lifetimes for these two cases were 12 and 70 min, respectively. The resulting daytime model generated H_2SO_4 concentrations as shown in Fig. 4. In model 3 a shift in the total aerosol surface from 75 to 13 $\mu m^2/cm^3$ was invoked to simulate a thin cloud dissipating into the BL air. These simulations show that the difference in H_2SO_4 concentrations depends linearly on the surface area difference. The 75 $\mu m^2/cm^3$ surface area scenario (thin cloud) results in $H_2SO_4(g)$ values well below those observed for out-of-cloud conditions, whereas the 13 $\mu m^2/cm^3$ surface area simulation approaches the observed maximum values. The model 3 simulation shows how fast $H_2SO_4(g)$ could potentially increase during midday hours after a BL air parcel is processed by clouds, given reasonably constant concentrations of SO_2. This rapid buildup of high concentrations of H_2SO_4 strongly favors heteromolecular nucleation. The spatial fluctuations in the observational data, in conjunction with the model simulation results, make a convincing case that the oxidation of marine-released DMS was the basis for the observed new BL aerosol formation.

To compare our observations with those predicted from classic nucleation theory we have used an approximation equation that expresses the critical concentration C_{crit} ($\mu g{\cdot}m^{-3}$) of $H_2SO_4(g)$ required to achieve a nucleation rate of $J = 1$ cm^{-3} (*28*). In making this comparison, we also assume that our 1.5-km spatial resolution reflects mean steady-state conditions.

$$C_{crit} = 0.16 \exp(0.1T - 3.5RH - 27.7) \quad (1)$$

Equation 1 predicts that when the ambient concentration C_s exceeds C_{crit}, the excess H_2SO_4 mass becomes available to form new

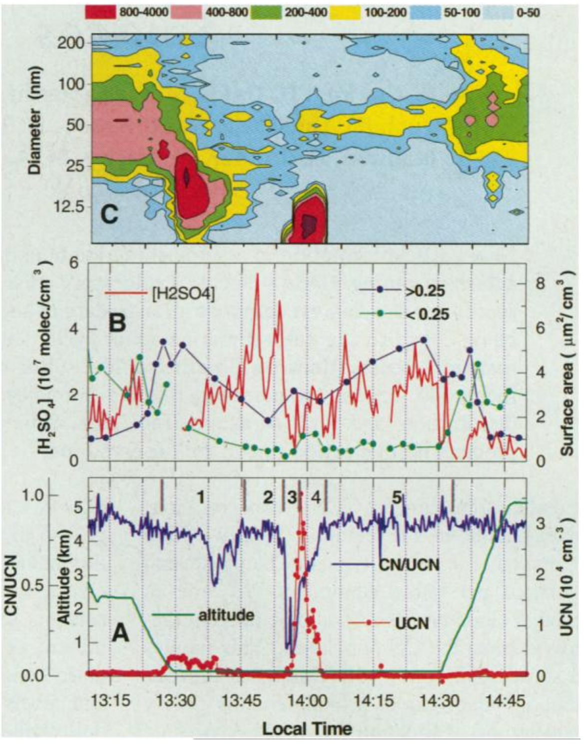

Fig. 1. (**A**) Five regions revealing different conditions for nucleation and characteristic UCN and CN/UCN ratios (*16*) during the flight 19 BL leg. Enhancements in small nuclei are revealed by the ratio of CN (Dp > 10 nm) to UCN (Dp > 3 nm). Region 1 has elevated UCN upon entering the BL at 13:23 hours that diminish after about 120 km, defining the new region 2 with low surface area and high $H_2SO_4(g)$ concentration. Very high concentrations of UCN indicate recent nucleation just before 14:00 hours (regions 3 and 4) followed by unusually low nuclei counts near 50 per centimeter (region 5), most likely due to scavenging by recent precipitation. [More typical equatorial BL values are in the range 300 to 400 per cubic centimeter (*1, 2, 10*)]. (**B**) Aerosol dry surface area for sizes above and below 0.25-µm and associated $H_2SO_4(g)$ concentrations. Estimated total wet surface areas (*17*) of 7 to 15 $\mu m^2/cm^3$ at 95% RH (about three times dry values) is smaller than all other BL values during PEMT (typically 30 to 200 $\mu m^2/cm^3$) and lowest before apparent active nucleation near 13:52 hours. The increase in small aerosol (Dp < 0.25 µm) surface area near 14:00 hours is from newly formed nuclei that account for about 0.7×10^7 molecules per cubic centimeter of $H_2SO_4(g)$ lost to this size range alone and consistent with the lower concentrations in this region. $H_2SO_4(g)$ is highest in region 2 (no detectable nucleation) and lowest in regions 3 (ongoing active nucleation) and 4 (aging nucleation event). (**C**) RDMA size distributions shown as concentration isopleths of diameter (logarithmic) versus time reveal a marked decrease at all sizes just before the region of active nucleation near 13:55 hours. The number peak near 60 nm seen above the BL on descent and ascent is also present in the BL but at much reduced concentrations because of scavenging. In region 5 populations of 60-nm particles are low and stable but increasing concentrations of 240-nm particles are primarily responsible for the increases in aerosol surface area (B) that can suppress nucleation.

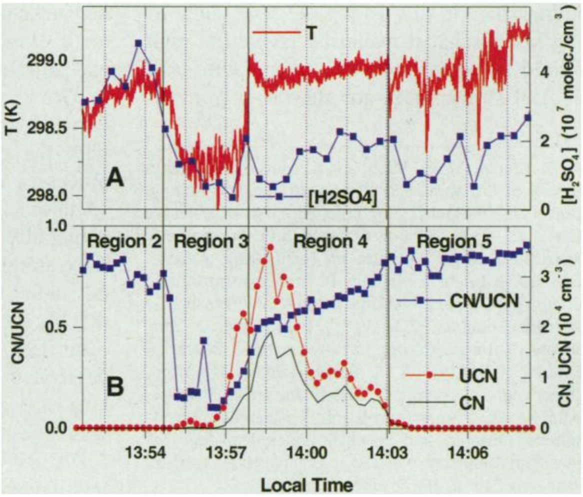

Fig. 2. (**A**) On this expanded scale for Fig. 1 temperatures drop to the lowest recorded during the BL leg, indicative of evaporative cooling associated with subsidence and probably related to the 15-s rain event at 13:56 hours. (**B**) Near 13.54 hours the CN/UCN ratio decreases to 0.15 within the 15-s averaging interval just as UCN start to increase. The CN/UCN ratio increases briefly to 0.4 and UCN decrease during the light rain event, indicating suppressed nucleation. Then the CN/UCN ratio drops to its lowest value before increasing to 0.5 at 13:58 hours and the UCN population increases rapidly, indicating steady increases in particle number and size in region 4.

particles. Thus, values for RH and T define C_{crit} for an air parcel that can be compared to the measured C_s. Higher altitudes (lower T) and near cloud conditions (high RH < 100%) with elevated $H_2SO_4(g)$ represent the most favored regions for nucleation. Within clouds (RH > 100%) measurements confirmed that the large increase in droplet surface area scavenges most available $H_2SO_4(g)$. However, the nonlinear dependence on RH and T caused by fluctuations within a near cloud environment can provide favorable conditions for nucleation (*29*). For air parcels of this type, the highest observed concentrations of $H_2SO_4(g)$ should approach the values needed for a potential nucleation event.

The subsiding air that supported the nucleation event near 14:00 hours we infer to lie between 0.3 and 1.3 km and probably near 0.6 km, as suggested by the highest UCN level observed on the initial descent at 8°N. In this case, the temperature should have been about 4°C lower than that at 160 m with RH near 98%. The variations in $H_2SO_4(g)$ at 0.6 km are assumed to be similar to those observed along the BL leg as revealed in the short horizontal leg flown at 2 km (Fig. 1A). The estimated C_{crit} for values of RH and T measured at 0.16, 0.6, and 1.3 km (Fig. 5) show that not even for the 1.3-km calculation does C_s approach C_{crit}. Shortfalls such as this have been noted (*14, 30*). Hence, these BL observations further demonstrate that classic binary nucleation theory cannot be applied without the use of a significant tuning factor. This may point to a deficiency in classic theory as applied to the current setting or possibly to the existence of alternative mechanisms for nucleation. The latter might include ternary nucleation involving ammonia emitted from the ocean surface (*31–35*) or the possibility that nucleation occurred on ions, because heavy lightning activity was observed during flight 19.

A final relevant issue concerns the time required between the formation of a critical H_2SO_4 cluster and the actual detection of UCN. This growth time can be approximated given a known surface area and measured quantities of $H_2SO_4(g)$ (*36*). Assuming a constant $H_2SO_4(g)$ concentration of 5×10^7 molecules per cubic centimeter (Fig. 1B), the minimum time to grow from a simple H_2SO_4/H_2O cluster to 3 nm would be 0.5, 1, and 2 hours, given possible $H_2SO_4(g)$ sticking coefficients (α) of 1, 0.7, and 0.3, respectively. Under our conditions (α = 0.6) about 1 or 2 hours would be required for $H_2SO_4(g)$ to recover after depletion from cloud processing and a similar amount of time would be required for nucleated aerosol to grow to a detectable size. Assuming that the BL is destroyed after a rain event and a nearly wet adiabatic temperature and moisture profile extends to the surface, we estimate from the observed moisture flux, that it should take 3 to 8 hours for the BL to recover to the height observed. Hence, sufficient time exists for the formation process. These observations also suggest that nucleation can take place for $H_2SO_4(g)$ levels in the BL that are nearly an order of magnitude less than required by classic nucleation theory, given the criteria of $J = 1\ \mathrm{cm}^{-3} \cdot \mathrm{s}^{-1}$.

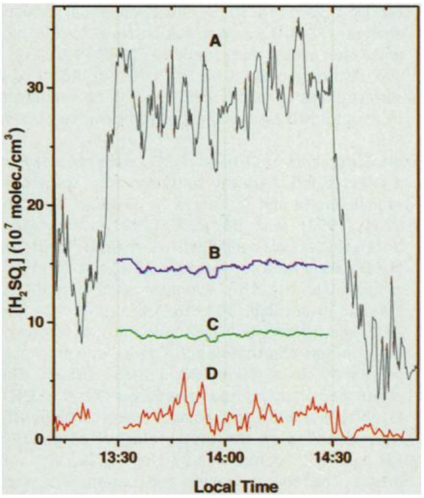

Fig. 5. Measured $H_2SO_4(g)$ and corresponding C_{crit} for ambient conditions at 160 m (**A**) and near cloud conditions at 600 m (a likely outflow region) (**B**) and at 1300 m (the highest outflow region consistent with O_3 data) (**C**). (**D**) Maximum measured $H_2SO_4(g)$ concentrations (the highest during any PEMT flight) lie well below the minimum possible C_{crit}.

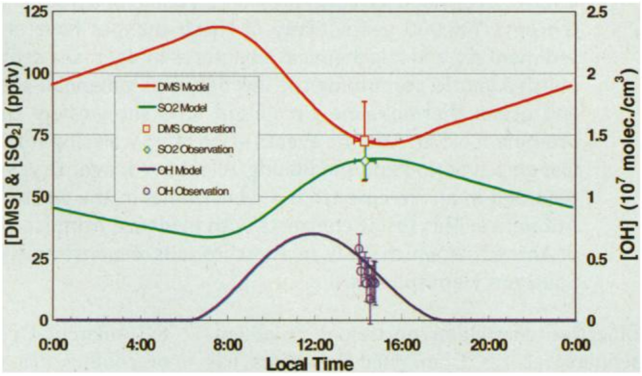

Fig. 3. DMS, SO_2, and OH model simulations for PEMT flight 19, 23 September 1996. The DMS flux was estimated at 5.7 micromolecules per square meter per day. The overall DMS/SO_2 conversion EF was 0.7 and the estimated first-order SO_2 loss was $1.3 \times 10^{-5}\ \mathrm{s}^{-1}$ (*20*). The OH profile was estimated from observed O_3 = 14.6 ppbv, NO = 11.5 parts per trillion by volume, CO = 71 ppbv, dew point = 23.6°C, and T = 296.5 K. All photolysis rates were reduced by 15% from the clear sky conditions reflecting the overhead cloud coverage.

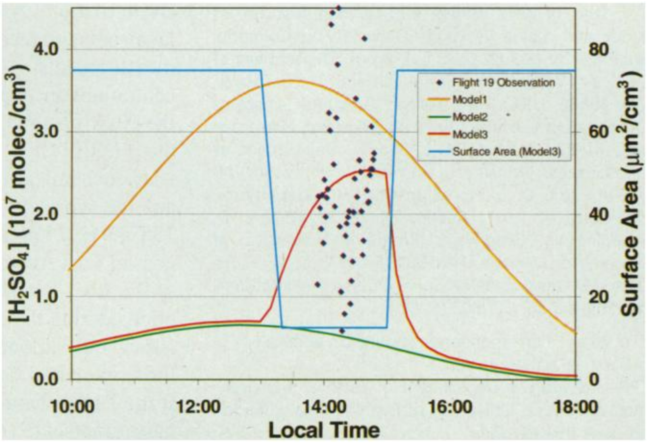

Fig. 4. Observed and model simulated H_2SO_4 for flight 19. Model simulations were based on model calculated SO_2 and OH 24-hour profiles constrained by boundary layer observations. Models 1 and 2 use fixed aerosol surface areas of 13 and 75 $\mu m^2/cm^3$, respectively. Model 3 simulates the effect of a sudden (<30 min) change in aerosol surface area on H_2SO_4 concentrations, corresponding to evaporating cloud boundaries.

References and Notes

1. A. D. Clarke, *J. Geophys. Res.* **92**, 4179 (1987).
2. D. S. Covert, V. N. Kapustin, T. S. Bates, P. K. Quinn, *ibid.* **101**, 6919 (1996).
3. B. Bonsang, B. C. Nguyen, A. Gaudry, G. Lambert, *ibid.* **85**, 7410 (1980).
4. M. O. Andreae and H. Raemdonck, *Science* **221**, 744 (1983).
5. R. J. Charlson, J. E. Lovelock, M. O. Andreae, S. G. Warren, *Nature* **326**, 655 (1987).
6. D. A. Hegg, L. F. Radke, P. V. Hobbs, *J. Geophys. Res.* **95**, 13917 (1990).
7. M. O. Andreae, S. J. de Mora, W. Elbert, *ibid.* **100**, 11335 (1995).
8. D. S. Covert, V. N. Kapustin, P. K. Quinn, T. S. Bates, *ibid.* **97**, 20581 (1992).
9. A. D. Clarke, *ibid.* **98**, 20633 (1993).
10. ———, Z. Li, M. Litchy, *Geophys. Res. Lett.* **23**, 733 (1996).
11. G. P. Ayers, J. P. Ivey, R. W. Gillet, *Nature* **349**, 404 (1991).
12. X. Lin, W. L. Chameides, C. S. Kiang, A. W. Stelson, H. Berresheim, *J. Geophys. Res.* **97**, 18161 (1992).
13. G. E. Shaw, *Atmos. Environ.* **23**, 2053 (1989).
14. F. Raes, *J. Geophys. Res.* **100**, 2893 (1995).
15. National Research Council, *Aerosol Radiative Forcing and Climate Change* (National Academy Press, Washington, DC, 1996), p. 48.
16. Major aerosol instruments consisted of CN with diameters Dp > 10 nm (TSI 3760), UCN with diame-

ters Dp >3 nm (TSI 3025), radial differential mobility analyzer (RDMA) size distribution Dp 8 to 250 nm, and a laser optical particle counter (OPC-PMS LAS-X) size distribution Dp, 150 to 7000 nm. RDMA dry surface areas at about 25% RH can be multiplied by about 3 to estimate ambient surface areas at 94% RH.

17. Measurements of OH and H_2SO_4 were recorded on a selected-ion chemical-ionization mass spectrometer [F. Eisele and D. Tanner, *J. Geophys. Res.* **96**, 9295 (1991); *ibid.* **98**, 9001 (1993)]. Two sigma uncertainties on individual 1-s measurements of H_2SO_4 are ±42% (precision is 20%) but are much reduced for the 15-s averages used here [R. L. Mauldin *et al.*, *ibid.* **101**, 16713 (1998)]. SO_2 and DMS measurements were made with an isotopic-dilution gas-chromatography mass spectrometer [A. Bandy *et al.*, *ibid.* **98**, 23423 (1993)]. The photochemically related parameters CO, H_2O, NO, O_3, NMHCs, and UV irradiance were continuously recorded as were the meteorological parameters RH and *T*; for details see (J. Hoell *et al.*, *ibid.*, in press). The above species and parameters were typically measured and averaged over times ranging from 15 s to 5 min. A subset of these (for example, vertical and horizontal winds, dew point, and temperature) was high-resolution 20-Hz data.
18. The time-dependent photochemical box model for diel trends in OH is similar to that described by D. Davis *et al.* [*J. Geophys. Res.* **101**, 211 (1996)] and J. Crawford *et al.* [*ibid.* **102**, 28447 (1997)]. The chemical model assumed all calculated species to be in photochemical equilibrium and included 50 standard HOx-NOx-CH_4 reactions, 118 NMHC reactions, 15 photolytic reactions, and heterogeneous removal of soluble species. It was constrained by input values for O_3, CO, CH_4, NMHCs, NO, H_2O, temperature, pressure, and, when available, measurements of the longer lived species H_2O_2, CH_3OOH, HNO_3, and peroxyacetyl nitrate. Photolysis rates were calculated with the National Center for Atmospheric Research community radiative transfer code configured for four-stream DISORT calculations. Calculated *J* values were scaled for cloud effects based on a comparison of the observed OH with model estimated values (typically 10%).
19. G. Chen *et al*, *J. Geophys. Res*, in press.
20. D. Davis *et al.*, *ibid.*, in press.
21. The DMS flux was estimated by using a mass conservation equation with measured DMS and OH values and model-generated diel profiles for NO_3—$d[\mathrm{DMS}]/dt = \mathrm{FDMS/EMD} - (\mathrm{kOH[OH]} + \mathrm{kNO_3}[\mathrm{NO_3}])[\mathrm{DMS}]$. The first term on the right-hand side is the DMS source term (sea-to-air flux), which depends on the oxidation rate of DMS and the equivalent mixing depth (EMD) (*19, 20*). The latter can be viewed as the height of an atmospheric column that contains all DMS mass (both buffer and boundary layers) but at BL concentrations. The DMS oceanic flux is balanced by a comparable loss by reaction with OH and NO_3 calculated from the 24-hour profiles for DMS, OH, and NO_3. For flight 19 the OH profile was generated independently from an O_3/HOx/NOx/CH_4 photochemical box model constrained both by the measured photochemical controlling parameters O_3, H_2O, CO, NO, NMHCs, UV, and *T* and by the limited in situ BL OH measurements (*18*). Evaluation of the EMD (1.3 km for flight 19) was based on the vertical concentration data for DMS and CH_3I (*17, 31*). Using our estimated BL height of 0.6 km, about half the DMS released had been transported into the overlying cloud layer and lower free troposphere.
22. S. Yvon *et al.*, *J. Geophys. Res.* **101**, 6899 (1996).
23. A. R. Bandy *et al.*, *Geophys. Res. Lett.* **23**, 741 (1996).
24. B. Huebert *et al.*, *J. Geophys. Res.* **98**, 16985 (1993).
25. T. Bates *et al.*, *ibid.* **92**, 2930 (1987).
26. The sulfur model used in this study is similar to that previously described (*17, 19, 31*) and is based on 14 sulfur reaction processes, five having two or more branches. Coupled sets of time-dependent continuity equations (with parameterized transport terms) are integrated to yield time-dependent concentration profiles of sulfur species. The general form of this equation is: $d[\mathrm{S}]_{\mathrm{BL}}/dt = Fsa/h + M/h \times ([\mathrm{S}]_{\mathrm{BuL}} - [\mathrm{S}]_{\mathrm{BL}}) + \mathrm{P(S)} - \mathrm{L(S)}[\mathrm{S}]_{\mathrm{BL}} - \mathrm{k(SL)}[\mathrm{S}]_{\mathrm{BL}}$. Here $[\mathrm{S}]_{\mathrm{BL}}$ represents the BL concentration of a given sulfur species (DMS, SO_2, MSA, H_2SO_4), $[\mathrm{S}]_{\mathrm{BuL}}$ is the concentration of the sulfur species in the buffer layer, *Fsa* is the sea-to-air flux of S (DMS), *h* is the marine BL height, *M* is the mixing parameter where $M = K/z$, P(S) is the photochemical production of sulfur species S, L(S) is the photochemical loss of sulfur species S, and k(SL) is the removal of S via aerosol (dry and wet) scavenging or dry deposition. The aerosol sticking coefficient for H_2SO_4 (*20*) was derived from data collected near Christmas Island in the tropical Pacific during P3-B mission 7 of PEMT.
27. D. Davis *et al.*, *J. Geophys. Res.* **103**, 1657 (1998).
28. A. S. Wexler, F. W. Lurmann, J. H. Seinfeld, *Atmos. Environ.* **28**, 531 (1994).
29. V. Kerminen and A. Wexler, *J. Geophys. Res.* **99**, 25607 (1994).
30. L. M. Russell, S. N. Pandis, J. H. Seinfeld, *ibid.*, p. 20989.
31. D. Davis *et al.*, Fall Meeting (American Geophysical Union, San Francisco, CA, 1997).
32. W. A. Hoppel, G. M. Frick, R. E. Larson, *Geophys. Res. Lett.* **13**, 125 (1986).
33. R. J. Weber *et al.*, *Chem. Eng. Commun.* **151**, 53 (1996).
34. A. D. Clarke and J. N. Porter, *J. Geophys. Res.* **98**, 16997 (1993).
35. P. K. Quinn, T. S. Bates, J. E. Johnson, D. S. Covert, R. J. Charlson, *ibid.* **95**, 16405 (1990).
36. The growth times for new nuclei over marine regions have been shown (*37*) to be inversely proportional to H_2SO_4(g) and α. It was also shown that for a fixed H_2SO_4(g) source strength the growth rate is independent of α because H_2SO_4(g) is inversely proportional to α. Because H_2SO_4(g) and its variation at the time of nucleation is unknown we have used a range of α to provide a plausible range of growth times.
37. W. A. Hoppel, G. M. Frick, J. W. Fitzgerald, R. E. Larson, *J. Geophys. Res.* **99**, 14443 (1994).

38. Supported by NASA grants NAG-1-1764 and NAG-1-1769. This is contribution 4687 from the School of Earth Science and Technology, University of Hawaii.

9 June 1998; accepted 27 August 1998

Synchronous Climate Changes in Antarctica and the North Atlantic

E. J. Steig,*† E. J. Brook, J. W. C. White, C. M. Sucher, M. L. Bender, S. J. Lehman, D. L. Morse, E. D. Waddington, G. D. Clow

Central Greenland ice cores provide evidence of abrupt changes in climate over the past 100,000 years. Many of these changes have also been identified in sedimentary and geochemical signatures in deep-sea sediment cores from the North Atlantic, confirming the link between millennial-scale climate variability and ocean thermohaline circulation. It is shown here that two of the most prominent North Atlantic events—the rapid warming that marks the end of the last glacial period and the Bølling/Allerød–Younger Dryas oscillation—are also recorded in an ice core from Taylor Dome, in the western Ross Sea sector of Antarctica. This result contrasts with evidence from ice cores in other regions of Antarctica, which show an asynchronous response between the Northern and Southern Hemispheres.

Objective correlation of isotope paleotemperature records from polar ice cores has shown that some climate variations once thought to be synchronous in both hemispheres are in fact out of phase. For example, the Antarctic Cold Reversal (ACR), a period of cooling that appears in many Antarctic stable isotope records (*1*), has been compared with the Younger Dryas (YD), a prominent feature in Northern Hemisphere records (*2*). Time series for the cores from Vostok and Byrd Station, Antarctica, correlated to the layer-counted records in central Greenland by measurements of atmospheric trace gas concentrations in trapped air bubbles, show that the ACR occurred at least 1000 years before the YD (*3, 4*).

Geochemical climate proxies (*5, 6*) from an ice core at Taylor Dome (77°48′S, 158°43′E, 2374 m above sea level), a near coastal East Antarctic site at the western edge of the Ross Sea (Fig. 1), exhibit large fluctuations during the last glacial-interglacial transition and Holocene that are reminiscent of those in central Greenland. Published records from Taylor Dome, however, use a preliminary time scale (*6*) that precludes definitive

---

E. J. Steig, J. W. C. White, S. J. Lehman, Institute of Arctic and Alpine Research, University of Colorado, Boulder, CO 80309, USA. E. J. Brook, Department of Geology, Washington State University, Vancouver, WA 98686, USA. C. M. Sucher, Graduate School of Oceanography, University of Rhode Island, Narragansett, RI 02882, USA. M. L. Bender, Department of Geosciences, Princeton University, Princeton, NJ 08544, USA. D. L. Morse, Institute for Geophysics, University of Texas, Austin, TX 78759, USA. E. D. Waddington, Geophysics Program, University of Washington, Seattle, WA 98195, USA. G. D. Clow, United States Geological Survey, Denver Federal Center, Englewood, CO 80225, USA.

*To whom correspondence should be addressed. E-mail: steig@colorado.edu

†Present address: Department of Earth and Environmental Science, University of Pennsylvania, Philadelphia, PA 19104, USA.